American Journal of Pathology, Vol. 152, No. 1, January 1998

Expression and Location of Pro-Apoptotic Bcl-2 Family Protein BAD in Normal Human Tissues and Tumor Cell Lines

Shinichi Kitada,* Maryla Krajewska,* Xin Zhang,* Dominic Scudiero,† Juan M. Zapata,* Hong-Gang Wang,* Ahmed Shabaik,‡ Gabriella Tudor,† Stanislaw Krajewski,* Timothy G. Myers,§ George S. Johnson,§ Edward A. Sausville,§ and John C. Reed*

From the Burnham Institute, Cancer Research Center, La Jolla, and the Department of Pathology,‡ University of California at San Diego, San Diego, California, and the National Cancer Institute–Frederick Cancer Research and Development Center,† Frederick, and the National Cancer Institute Developmental Therapeutics Program,§ Bethesda, Maryland*

The BAD protein is a pro-apoptotic member of the Bcl-2 family whose ability to heterodimerize with survival proteins such as Bcl-X_L and to promote cell death is inhibited by phosphorylation. Monoclonal antibodies were generated against the human BAD protein and used to evaluate its expression by immunoblotting and immunohistochemistry in normal human tissues and by immunoblot analysis of the National Cancer Institute anti-cancer drug screening panel of 60 human tumor cell lines. BAD protein was detectable by immunoblotting in many normal tissues, with testis, breast, colon, and spleen being among those with the highest steady-state levels. Immunostaining of tissues revealed many examples of cell-type-specific expression of BAD, suggesting dynamic regulation of BAD protein levels *in vivo*. In many types of normal cells, BAD immunoreactivity was associated with cytosolic organelles resembling mitochondria, suggesting that BAD is often heterodimerized with other Bcl-2 family proteins *in vivo*. The relative levels of BAD protein varied widely among established human tumor cell lines, with colon, lung, and melanomas generally having the highest expression. As a group, hematopoietic and lymphoid lines contained the least BAD protein. The BAD protein derived from 11 of 41 tumor lines that expressed this pro-apoptotic protein migrated in gels as a clear doublet, consistent with the presence of hyperphosphorylated BAD protein. Taken together, these findings define for the first time the normal cell-type-specific patterns of expression and intracellular locations of the BAD protein *in vivo* and provide insights into the regulation of this pro-apoptotic Bcl-2 family protein in human tumors. ***(Am J Pathol 1998, 152:51–61)***

Dysregulation of programmed cell death (PCD) can play an important role in the pathogenesis of many human malignancies through several mechanisms, including 1) prevention of the normal programmed turnover of cells, 2) blockage of apoptosis induced by activated oncogenes such as Myc and Cyclin-D1, 3) prevention of cell death triggered by genomic aberrations and DNA damage (ie, promoting genetic instability), and 4) interference with apoptosis induced by loss of cell attachment to the extracellular matrix, potentially contributing to metastasis (reviewed in Refs. 1–3). Among the important regulators of PCD and apoptosis are the Bcl-2 family of proteins. These proteins control a distal step in an evolutionarily conserved pathway for cell death, with some functioning as blockers and others as promoters of cellular demise.[1,4]

The BAD protein is a pro-apoptotic member of this family that can bind to anti-apoptotic proteins, including Bcl-2 and Bcl-X_L.[5,6] The BAD protein contains two PEST sequences,[5] suggesting that it may be relatively short-lived, but lacks the carboxyl-terminal membrane-anchoring domain found in many Bcl-2 family proteins. Recent data indicate that BAD can become phosphorylated at one or two serine residues, resulting in its dissociation from Bcl-2 and Bcl-X_L and its sequestration by cytosolic 14-3-3 family proteins.[7] As Bcl-2 and Bcl-X_L are anchored in mitochondrial and some other types of intracellular membranes, with the bulk of these proteins oriented toward the cytosol, phosphorylation of BAD results in a translocation of this pro-apoptotic protein from the surface of these organelles to the cytosol. The kinases responsible for inducing phosphorylation of BAD include Akt, which is activated by the phosphatidylinositol 3′-kinase (PI3K) pathway,[8] and Raf-1, which can be targeted to mitochondria through its interactions with Bcl-2.[9]

Supported by funds provided by the Breast Cancer Fund of the State of California through the Breast Cancer Research Program of the University of California (grant 1RB-0093), by National Institutes of Health grant CA55164, and by an award from CaP-CURE, Inc.

Accepted for publication October 23, 1997.

Address reprint requests to Dr. Reed, The Burnham Institute, Cancer Research Center, 10901 North Torrey Pines Road, La Jolla, CA 92037. E-mail: jreed@burnham-institute.org.

Heretofore, the expression of the BAD protein had not been evaluated in either normal or neoplastic human cells, due in part to the absence of antibody reagents that specifically detect the human BAD protein. In this report, we describe the generation of monoclonal antibodies against BAD and present data concerning the expression of this pro-apoptotic protein in both normal human tissues and in a panel of 60 human tumor cell lines that have been used as part of a strategy at the National Cancer Institute for evaluating potential anti-cancer compounds.

Materials and Methods

Production of BAD protein and Monoclonal Antibodies

A glutathione S-transferase-human BAD (GST-hu-BAD) fusion protein was produced in bacteria and purified by affinity chromatography.[9] Transgenic mice that overexpress Bcl-2 in their B cells (line B6)[10] were immunized with GST-BAD protein, and splenocytes were fused with SP/2 cells to generate hybridomas as described previously.[11] Positive hybridomas were identified by a primary enzyme-linked immunosorbent assay (ELISA) screening assay using GST-BAD protein, followed by a secondary ELISA screen using GST protein to eliminate clones producing anti-GST antibodies. Cells from two positive wells were subcloned twice, and the resulting hybridomas were used for monoclonal antibody production as ascites in pristane-primed BALB/c mice.[11] Both hybridomas (P1C2 (subclone A2.G3) and P3F6 (subclone A5.A6)) were determined to secrete IgG_1 murine immunoglobulins.

Immunoblotting

Whole-cell lysates were prepared from frozen human tissues obtained at autopsy, normalized for total protein content, and subjected to sodium dodecyl sulfate polyacrylamide gel electrophoresis (SDS-PAGE)/immunoblot assay as described previously,[12–14] using 0.1% (v/v) anti-BAD monoclonal P1C2 (subclone A2.G3) ascites and an enhanced chemiluminescence (ECL) detection method. Analysis of cell lines was performed in the same way, except phosphatase inhibitors were added to the lysis solution (5 mmol/L NaF, 2 mmol/L sodium orthovanadate, 10 mmol/L sodium β-glycerol phosphate, 2 mmol/L sodium pyrophosphate, 50 mmol/L *p*-nitrophenylphosphate, and 1 μmol/L cystin LR), along with the usual protease inhibitors (1 mmol/L phenylmethylsulfonyl fluoride, 0.28 trypsin inhibitor units/ml aprotinin, 50 μg/ml leupeptin, 1 mmol/L benzamidine, 0.7 μg/ml pepstatin). After collecting data for the entire 60-cell panel on immunoblot filters, residual lysates from two representative tumor lines per blot were re-analyzed together in the same blot along with a standard curve created by using (1 to 20 ng per lane) GST-BAD protein. Data on x-ray films were quantified by scanning densitometry using the IS-1000 image analysis system (Alpha Innotech Co., San Leandro, CA), and the results from the GST-BAD standard-containing blot were used to normalize all data before estimating the nanograms of BAD protein per 50 μg of total protein. Data from two independent GST-BAD standard-containing blots were within 20% agreement.

Immunohistochemistry

For immunohistochemical assays, tissues were fixed in either neutral-buffered formalin, zinc-buffered formalin (Z-fix, Anatech, Battle Creek, MI), or Bouin's solution (Sigma Chemical Co., St. Louis, MO), embedded in paraffin, sectioned (5 μm), and immunostained using diaminobenzidine-based detection methods in conjunction with either an avidin-biotin or a streptavidin-biotin enhancement system (LSAB+ kit, Dako, Santa Barbara, CA), as described in detail.[12–14] The anti-BAD monoclonals were used as ascites at a 1:100 to 1:600 dilution. The secondary antibody in the avidin-biotin complex system was 2.0 μg/ml horse biotinylated immunoglobulins directed against mouse IgG and was followed by horseradish peroxidase avidin-biotin complex reagent (Vector Laboratories, Burlingame, CA). LSAB+ reagents were used in the original concentrations provided by the manufacturer. Nuclei were counterstained with hematoxylin. For all tissues examined, the immunostaining procedure was performed in parallel with omission of the primary antibody or after incubation with irrelevant, mouse immunoglobulins (Dako), thus providing a control for immunospecificity. The immunostaining results were arbitrarily scored for both the cytosolic and organellar components according to intensity as follows: 0, negative; 1+, weak; 2+, moderate; 3+, strong. All results were derived from a minimum of five independent autopsy or biopsy specimens.

Results

Characterization of Anti-BAD Monoclonal Antibodies

Using GST-BAD as an immunogen, two monoclonal antibodies were successfully generated that displayed reactivity in ELISAs with GST-BAD but not GST protein. Immunoblot analysis confirmed that these monoclonal antibodies reacted specifically with GST-BAD but not GST (Figure 1A and data not shown). The specificity of these monoclonal antibodies for the BAD protein was further demonstrated by comparisons with other GST fusions representing additional members of the Bcl-2 protein family. As shown in Figure 1A, the anti-BAD monoclonal antibody P1C2 failed to react with GST-Bcl-2, GST-Bcl-X_L, GST-Bax, or GST-Bak. Similar results were obtained for the monoclonal antibody P3F6 (not shown).

To determine whether these monoclonal antibodies were capable of reacting with BAD protein produced in mammalian cells, immunoblot analysis was performed using lysates prepared from 293T cells that had been transfected with a plasmid encoding FLAG-BAD or a control plasmid (pcDNA-3). As shown in Figure 1B, both

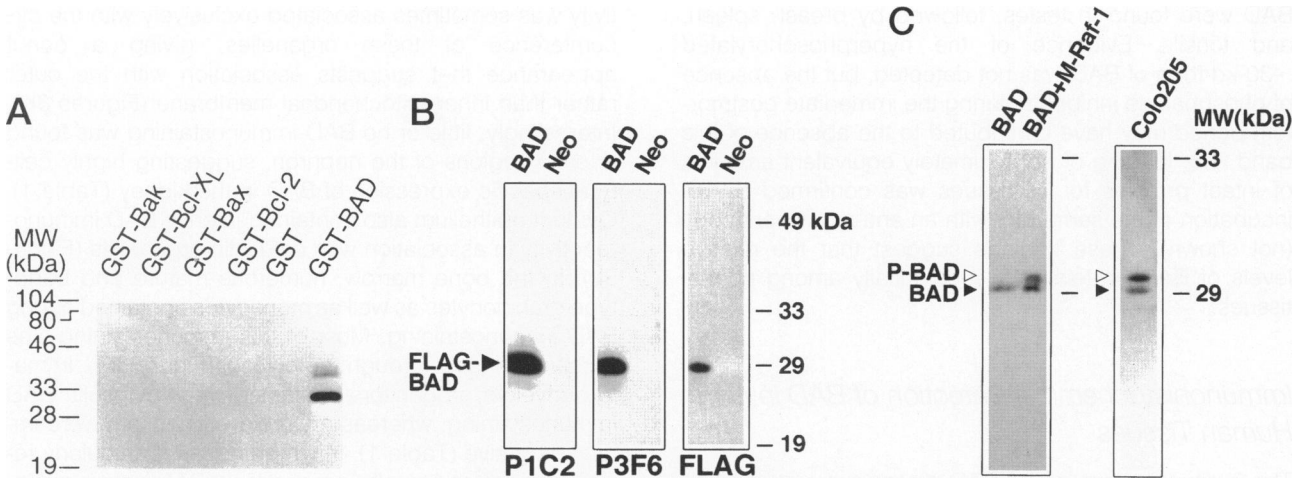

Figure 1. Characterization of anti-BAD monoclonal antibodies. **A:** GST and various GST-fusion proteins, which were produced in bacteria and affinity purified,[9] were analyzed by SDS-PAGE/immunoblot assay (50 ng per lane) using anti-BAD monoclonal P1C2 with ECL-based detection. The major band seen represents a partial proteolytic degradation fragment of GST-BAD. **B:** 293T cells were transiently transfected with pcDNA3 or pcDNA3-FLAG-BAD as described,[9] and cell lysates (50 μg per lane) were analyzed by SDS-PAGE/immunoblot assay, where pairs of control (Neo) and FLAG-BAD-expressing (BAD) lysates were run in triplicate. The blot was then cut into three sections and incubated with the anti-BAD antibodies P1C2 or P3F6 or with an anti-FLAG antibody. **C:** 293T cells were co-transfected with pcDNA3-BAD in combination with either pcDNA3-M-Raf-1 or an equivalent amount of pcDNA3 control vector as described.[9] Lysates (50 μg per lane) were prepared in the presence of phosphatase inhibitors, and immunoblot assays were performed using either the P1C2 or P3F6 antibody. For comparison, immunoblot analysis of a lysate from Colo205 cells is shown. The relative positions of the BAD and hyperphosphorylated BAD proteins are indicated by **solid** and **open arrows**, respectively.

antibodies reacted with the FLAG-BAD protein, as did the anti-FLAG monoclonal antibody M2.

As the hyperphosphorylated form of BAD has been reported to be ineffective as a promoter of apoptosis, it was important to know whether these anti-BAD monoclonals retained reactivity with the BAD protein when phosphorylated. To this end, phosphorylation of BAD was induced by expressing a mitochondria-targeted active version of the kinase Raf-1 (M-Raf-1) in 293T cells.[9] These cells were determined by immunoblotting to contain relatively high levels of endogenous human BAD protein. Cell lysates derived from M-Raf-1-expressing and control transfected 293T cells were then subjected to SDS-PAGE/immunoblot analysis using anti-BAD monoclonal antibodies. As shown in Figure 1C, the P1C2 monoclonal antibody reacted with two proteins that migrated as a doublet of ~ 29 and ~ 30 kd when lysates were prepared from M-Raf-1-expressing cells, whereas only a single band of ~29 kd was detected for control cells. Similar results were also obtained for the P3F6 antibody (not shown). Additional studies in which these lysates were treated with phosphatases confirmed that the slower-migrating protein represented phosphorylated BAD[9] (and data not presented). These two bands detected by anti-BAD monoclonals in lysates from M-Raf-1-expressing 293 cells also co-migrated in gels with the endogenous protein bands seen in certain tumor lines such as Colo205, further supporting the idea that the anti-BAD monoclonal antibodies generated here are capable of reacting with both unphosphorylated and hyperphosphorylated BAD protein (Figure 1C).

Immunoblot Detection of BAD Protein in Normal Human Tissues

Lysates prepared from various human tissues obtained at autopsy were normalized for total protein content and subjected to SDS-PAGE immunoblot analysis. The anti-BAD monoclonal P1C2 was arbitrarily chosen for this and all subsequent studies. At least low levels of the expected ~29-kd BAD protein were detected in nearly all tissues examined (Figure 2). The highest steady-state levels of

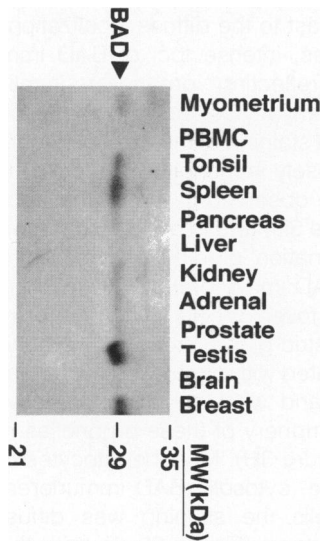

Figure 2. BAD protein expression in normal human tissues. Lysates prepared from human tissues obtained at autopsy were normalized for total protein content (50 μg per lane) and subjected to immunoblot assay using the P1C2 monoclonal antibody.

BAD were found in testes, followed by breast, spleen, and tonsils. Evidence of the hyperphosphorylated ~30-kd form of BAD was not detected, but the absence of phosphatase inhibitors during the immediate postmortem period may have contributed to the absence of this band. The loading of approximately equivalent amounts of intact proteins for all tissues was confirmed by reincubation of the same blot with an anti-tubulin antibody (not shown). These findings suggest that the relative levels of BAD protein vary substantially among normal tissues.

Immunohistochemical Detection of BAD in Human Tissues

The *in situ* locations of the BAD protein were studied by an immunohistochemical approach using paraffin-embedded human tissues. In many types of cells, BAD immunoreactivity was clearly associated with discrete cytosolic organelles resembling mitochondria. Table 1 summarizes the results for all human tissues, and Figure 3 shows some representative immunostaining results, emphasizing a few of the more salient features of BAD immunostaining. The specificity of all immunostaining results was confirmed by performing the procedure using a negative control murine antibody on adjacent tissue sections.

Overall, the expression of BAD *in vivo* is more restricted than previously observed for most other members of the Bcl-2 family and displays a highly tissue-specific distribution. As shown in Figure 3A, BAD immunostaining in the keratinocytes of the epidermis was localized diffusely through the cytosol. Interestingly, the intensity of BAD immunoreactivity was lower in the long-lived basal cell layer of keratinocytes located along the basement membrane compared with the more differentiated cells that migrate toward the body surface, implying a potential role for BAD in promoting apoptosis in differentiated keratinocytes. In contrast to the diffuse localization of BAD seen in keratinocytes, intense foci of BAD immunoreactivity (presumably reflecting organellar localization) were found in cardiomyocytes and smooth muscle cells, along with some faint staining of the cytosol (Figure 3, B and C). Similarly, intensely immunostained foci of BAD immunoreactivity were observed in the epithelial cells lining the trachea (Figure 3D) and in aveolar macrophages (Figure 3E). A combination of diffuse cytosolic and punctate perinuclear BAD immunoreactivity was found in the mucin-producing foveolar cells lining the gastric pits (Figure 3F). In the gastric glands, the BAD immunostaining was mostly associated with organelles with the appearance of mitochondria and with the immunoreactivity enhanced around the periphery of these organelles rather than inside them (Figure 3H). Most hepatocytes contained discrete, punctate, cytosolic BAD immunoreactivity, but in occasional cells the staining was diffusely localized through the cytosol (Figure 3I). In both the acinar pancreas and distal collecting tubules of the kidney, BAD immunoreactivity was mostly associated with what appeared to be mitochondria. Moreover, the immunoreactivity was sometimes associated exclusively with the circumference of these organelles, giving a donut appearance that suggests association with the outer rather than inner mitochondrial membrane (Figures 3K). Interestingly, little or no BAD immunostaining was found in other regions of the nephron, suggesting highly cell-type-specific expression of BAD in the kidney (Table 1). Oviduct epithelium also contained intense BAD immunoreactivity in association with cytosolic organelles (Figure 3L). In the bone marrow, numerous mature and band-type granulocytes as well as monocytes contained strong BAD immunostaining. Most of this immunostaining was present diffusely through the cytosol (Figure 3M). Immature myeloid progenitors contained weak cytosolic BAD immunostaining, whereas erythroid progenitors were immunonegative (Table 1). In lymph nodes, particularly reactive nodes and tonsils, predominant BAD immunostaining was identified in plasma cells, but small round lymphocytes were completely immunonegative, and large activated lymphocytes contained no or only faint BAD immunostaining (Figure 3O). The BAD immunostaining in plasma cells was primarily present diffusely through the cytosol, although a component of the immunoreactivity took on a granular quality suggestive of organelle association. In the brain, only occasional neurons were BAD immunopositive, with the immunostaining invariably associated with what appeared to be mitochondria. However, the paraspinal dorsal root ganglionic cells contained strong BAD immunoreactivity that was clearly associated with mitochondria. The BAD immunostaining of these organelles was localized mostly to the circumference, giving the same donut appearance seen in several other types of cells and again suggesting association of BAD with the outer mitochondria membrane (Figure 3Q).

Immunoblot Analysis of BAD Protein in the National Cancer Institute 60-Tumor-Cell-Line Screening Panel

Lysates were prepared in the presence of phosphatase and protease inhibitors from the National Cancer Institute 60-cell-line anti-cancer drug screening panel. After normalization for total protein content (50 μg per lane), samples were subjected to immunoblot analysis using the anti-BAD monoclonal antibody P1C2. Figure 4 shows a representative example of some immunoblot data, demonstrating a range of BAD protein levels in the tumor lines and showing that the BAD protein occasionally migrated as doublet (consistent with the presence of both unphosphorylated and hyperphosphorylated BAD) using lysates prepared from certain cell lines such as SK-MEL28 and UACC-257.

Table 2 summarizes the anti-BAD immunoblot results for all 60 tumor cell lines. Note that several colon and lung cancer lines within this panel contained relatively higher levels of BAD protein (>0.2 ng/ug), as did some melanomas and the prostate cancer line Du145. Among the various tumor lines tested, hematopoietic and lymphoid lines generally contained the lowest amounts of BAD

Table 1. BAD Immunoreactivity in Normal Human Tissues

Organ/tissue	Structure/cell type	BAD intensity	
		Organelles	Cytosol
Skin			
Epidermis	Keratinocytes		
Stratum basale	Basal cell layer	0	1+
Stratum spinosum	Spinous layer	0	2–3+
Stratum granulosum	Granular layer	0	3+
Stratum corneum	Cornified layer	0	1–2+
Dermis			
Stroma	Fibroblasts	0	0–1+
Sweat gland	Epithelium	0	1–2+
Sabaceous gland	Epithelium	0	1+
Musculoskeletal			
Cartilage	Chondrocytes	0	0–3+
	Fibroblasts	0	0
Bone	Osteocytes	0	1–2+
	Osteoclasts	NF	
Striated Muscles	Muscle fibers	2+	0–1+
Cardiovascular			
Heart			
Myocardium	Myocytes	2–3+	1+
	Capillary endothelium	0	0–2+
Arteries	Endothelial cells	0	0–2+
	Smooth muscle cells	2–3+	0–1+
	Fibroblasts	0	0
Respiratory system			
Trachea			
Epithelium (pseudostratified columnar)	Basal cell layer	0	2–3+
	Luminal cell layer	2+	1+
Submucosa	Fibroblasts	0	0
	Smooth muscle cells	1–2+	0–1+
	Sero-mucous glands	0	0–2+
Cartilage	Chondrocytes	0	0–2+
Lungs			
Bronchi			
Pseudostratified or simple columnar epithelium		3+	0
Alveoli	Type I pneumocytes	0	0
	Type II pneumocytes	0	0
	Alveolar macrophages	3+	0
Alimentary tract			
Salivary gland (submandibular gland)			
Secretory gland acini	Serous cells	0	0–2+*
	Mucous cells	0	0
	Salivary duct epithelium	0–2+*	0
Esophagus			
Stratified squamous epithelium	Basal cell layer	0	1+
	Spinous layer	0	1–2+
	Granular layer	0	1–2+
Muscularis externa	Smooth muscle cells	1–2+	0–1+
Stomach			
Cardiac region	Gastric pits/foveolar cells	2–3+	1+
	Cardiac glands	2–3+	0–1+
Submucosal plexus (Meissner's plexus)	Ganglion cells	0	0
Small intestine	Absorptive epithelium	0	1+
	Paneth cells	0	0
Colon	Absorptive cells	1–2+	0–1+
	Goblet/mucous cells	1+	0–1+
	Smooth muscle cells	2–3+	0–1+
Liver	Hepatocytes	2–3+	0–1+
	Sinusoidal endothelium	0	0
	Bile duct epithelium	1+	0–1+
Pancreas			
Exocrine	Acinar cells	0–3+	0
	Ductal epithelium	1–2+	0–1+
Endocrine	Islets of Langerhans	0–2+*	0

Immunostaining was located both in cytosol or cell organelles and was scored as follows: 0, immunonegative; 1+, weakly positive; 2+, moderate intensity; 3+, strong intensity of immunostaining. Results are reflective of combined data from a minimum of five autopsies or biopsies. NF, not found (ie, not present).
*Occasional scattered immunopositive cells.

Table 1. Continued

Organ/tissue	Structure/cell type	BAD intensity	
		Organelles	Cytosol
Urinary			
Kidney			
Glomeruli	Mesangial cells	0	0
Bowman's capsule	Parietal layer/squamous epithelium	0	0–1+
	Visceral layer/podocytes	0	0–1+
Collecting tubules	Proximal convoluted tubules	0	0–1+
	Loop of Henle-thin limb	0–2+	0
	Distal convoluted tubules	0–3+	0
Collecting ducts	Epithelial cells	0–1+	0–1+
Urinary bladder	Transitional epithelium	0	1–3+
Reproductive			
Male			
Testis	Leydig cells	0	0
	Sertoli cells	0	0–2+*
	Spermatogonia	0	0–3+*
	Spermatocytes	0	0
	Spermatids	0	0
	Spermatozoa	0	0
Prostate			
Tubuloalveolar glands	Basal cells	0	0
	Luminal secretory cells	0	0
Fibromuscular stroma	Smooth muscle cells	0	0
	Fibroblasts	0	0
Female			
Uterus			
Endometrium	Simple columnar epithelium	1–2+	0
	Stromal cells	0	0
Myometrium	Smooth muscle cells	0–1+	0
Ovary			
Primary follicles	Oocyte	NF	
	Follicular cells		
Secondary follicles	Granulosa cells	0	0
	Theca interna cells	0	0
	Theca external cells	0	0
Corpus luteum	Granulosa lutein cells	0	0
	Theca lutein cells	0	0
Oviduct (Fallopian tube)			
Mucosa	Ciliated columnar epithelium	2–3+	0–1+
	Secretory cells	0	0
Muscularis	Smooth muscle cells	0–1+	0
Mammary gland			
Tubuloalveolar glands	Cuboidal/columnar epithelium	1+	1–2+
Lactiferous ducts	Columnar epithelium	1+	1–2+
	Myoepithelial cells	0	1–2+
Loose/fibrous stroma	Fibroblasts	0	0
Hematolymphoid system			
Thymus			
Cortex	Cortical thymocytes	0	0
	Macrophages (dendritic, interdigitating cells)	0	0
Medulla	Epithelioreticular cells	0	0
	Hassall's corpuscles	0	0
	Medullary thymocytes	0	0
Tonsil/lymph nodes			
Germinal center	Large noncleaved cells	0	0
	Small noncleaved cells	0	0
	Small cleaved cells	0	0
	Follicular dendritic cells	0	0
	Macrophages	0	0
Mantle zone	Lymphocytes	0	0
Interfollicular region	Small lymphocytes	0	0
	Large transformed lymphocytes	0	0
	Sinus histiocytes	0	0
	Plasma cells	0	2–3+
Spleen			
Periarteriolar sheets	B lymphocytes	0	0
Marginal zone	T lymphocytes	0	0
Red pulp	Granulocytes	0	0–2+
	Erythrocytes	0	0

Table 1. Continued

Organ/tissue	Structure/cell type	BAD intensity	
		Organelles	Cytosol
Bone Marrow	Erythroid precursors	0	0
	Myeloid precursors	0	0–1+
	Megakaryocytes	0	0–2+
	Mature neutrophils	1–2+	2–3+
	Plasma cells	0	1–3+
	Monocytes	0	0–3+
Peripheral blood	Granulocytes	1–3+	1–3+
	Monocytes	0	0–2+
	Lymphocytes	0	0
	Erythrocytes	0	0
Central nervous system			
Cortex and basal ganglia			
Gray matter	Normal neurons	1–2+*	0–1+*
	Axons	0	0–1+
	Neuropil	0	0–1+
White matter	Myelin sheath	0	0
Neuroglia	Astrocytes	0	0
	Oligodendroglia	0	0
Microglia	Resting	0	0
	Activated	0–2+	0
Ependyma	Ependymal cells	0	1+
Leptomeninges	Arachnoid epithelium	0	1+
Choroid plexus	Epithelium	1–3+	1+
Cerebellum			
Cortex	Purkinje cells	0	0–1+*
	Granular cells	0	0
	Golgi cells	0	0
	Stellate and basket cells	0	0
	Astrocytes (Bergman glia)	0–2+	0
Medulla	Dentate nucleus	0	0
	Myelin fibres	0	0
Spinal cord			
White matter	Axons	0	0–1+
	Myelin sheath	0	0
Gray matter	Ventral horn motoneurons	0–1+*	0–1+*
	Dorsal horn sensory neurons	0–1+*	0–1+*
	Neuropil	0	0–1+
Peripheral nervous system			
Dorsal root and cranial nerve ganglia	Ganglion cells	0–3+	0
	Satellite cells	0	0
	Schwann cells	0	0
	Fibroblasts	0	0
Autonomic ganglia	Ganglion cells	0–2+	0
	Satellite cells	0	0
	Schwann cells	0	0
	Fibroblasts	0	0
Peripheral nerves	Axon	0	1–2+
	Myelin sheath	0	0
Endocrine system			
Thyroid	Follicle cells	0	0
Adrenal			
Cortex	Zona glomerulosa	0	0
	Zona fasciculata	0	0
	Zona reticularis	0	0
Medulla	Chromaffin cells	0	0
Adenohypophysis	Chromophobic cells	0	0
	Acidophilic cells	0	0
	Basophilic cells	0	0
Neurohypophysis	Nonmyelinated nerve fibers	0	0
	Glia	0	0

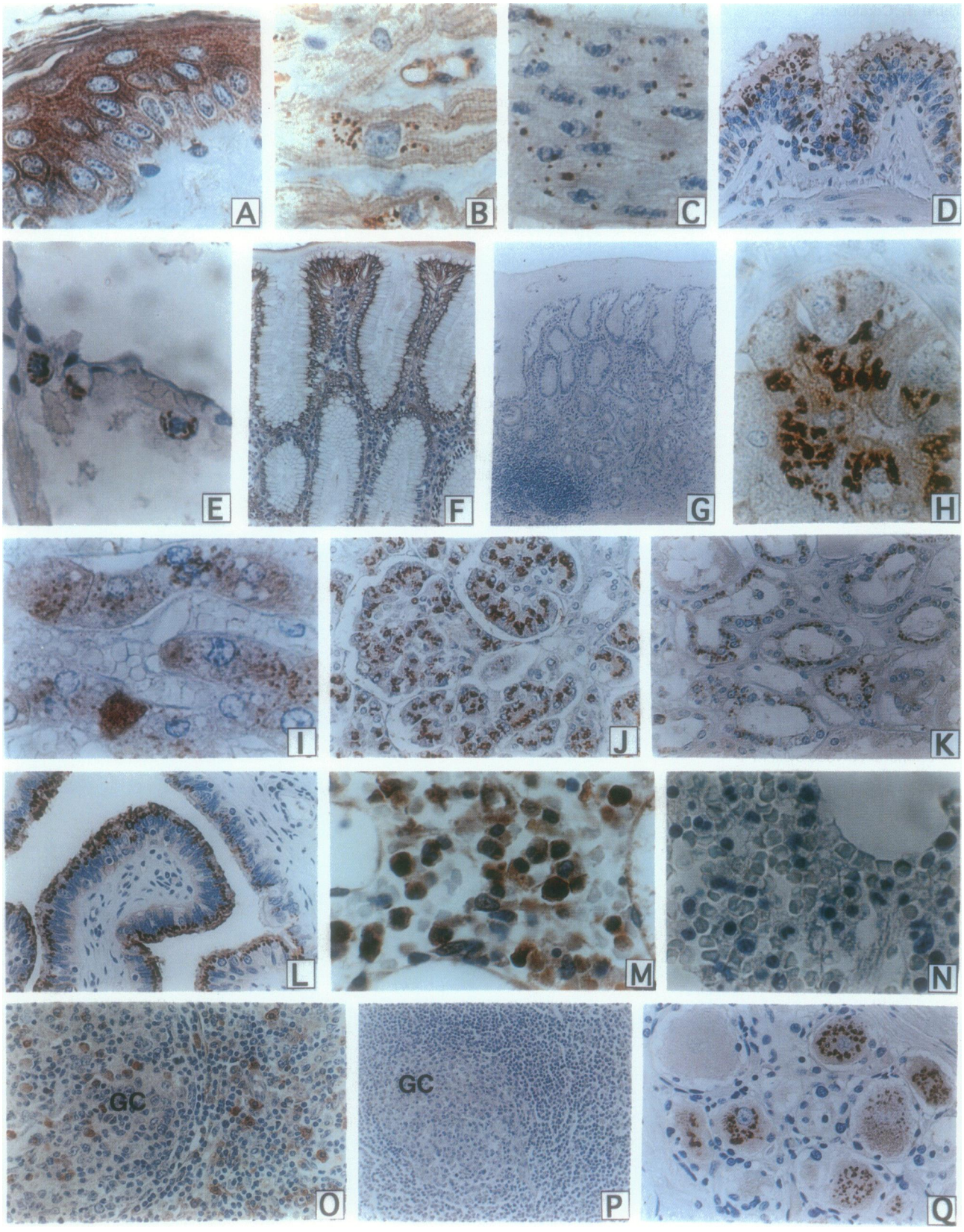
A
B
C
D
E
F
G
H
I
J
K
L
M
N
GC
O
GC
P
Q

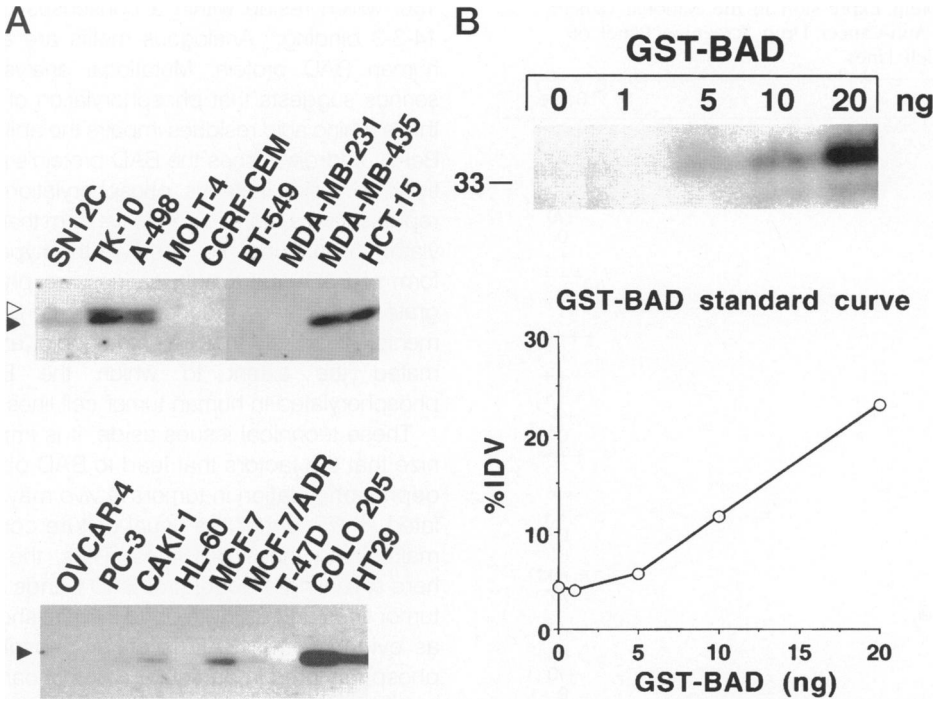

Figure 4. Examples of BAD protein expression in human tumor cell lines. **A:** Examples of immunoblot data are shown for several human tumor cell lines. In all cases, lysates were normalized for total protein content (50 μg) before SDS-PAGE/immunoblot assay using the P1C2 monoclonal antibody. The relative positions of the BAD and hyperphosphorylated BAD proteins are indicated by **solid** and **open arrows**, respectively. **B:** An example of a GST-BAD standard curve with densitometric quantification is presented (%IDV = percentage integrated density value), where 0 to 20 ng of purified GST-BAD protein was subjected to immunoblot analysis using an ECL-based detection method.

protein, with six of seven lines containing essentially no detectable BAD protein.

Statistical comparisons of BAD protein levels with other biochemical and molecular markers previously assessed in the 60-cell-line drug screening panel[15] revealed correlations between higher levels of BAD and DT-diaphorase activity ($r = 0.58$; $P < 0.0001$; n = 60), as well as with K-Ras mutations among lung and colon cancer cell lines ($r = 0.57$; $P = 0.02$; n = 16).

Discussion

Here we describe the generation of murine monoclonal antibodies that react specifically with the human BAD protein and demonstrate the application of these antibody reagents for analysis of BAD protein in normal tissues and human tumor cell lines by immunoblotting and immunohistochemistry. Recent studies indicate that the murine BAD protein can become phosphorylated at serines 112 and

Figure 3. Immunohistochemical analysis of BAD expression in normal tissues. Examples of BAD immunostaining in normal human tissues are provided. **A:** Epidermis, showing 1 to 2+ BAD immunostaining in the cytosol of the basal layer of keratinocytes with stronger intensity (3+) BAD immunoreactivity in the more differentiated keratinocytes in the upper layers of the epidermis. Original magnification, ×1000. **B:** Cardiomyocytes with punctate perinuclear staining and weak cytosolic staining, evidently associated with the sarcoplasma. ×1000. **C:** Smooth muscle cells from colon muscularis externa, showing strong punctate staining of cytosolic organelles. ×1000. **D:** Bronchial pseudostratified epithelium showing punctate organellar BAD immunostaining in epithelial cells but absence of BAD in underlying connective tissue fibroblasts. ×400. **E:** Alveoli showing strong organellar BAD immunoreactivity in aveolar macrophages but absence of BAD immunostaining in pneumocytes and endothelial cells. ×1000. **F:** Stomach, showing combination of strong intensity supranuclear organellar and modest intensity diffuse cytosolic BAD immunostaining in foveolar cells lining gastric pits. ×250. **G:** Negative control antibody (mouse IgG) staining of stomach from same individual. ×150. **H:** Gastric glands, demonstrating strong BAD immunoreactivity in association with what appear to be mitochondria in the mucoid cells. Note tendency of the BAD immunostaining to line the circumference of these organelles. ×1000. I: Liver, showing moderate intensity organellar BAD immunostaining in most hepatocytes, with an occasional cell having stronger diffuse cytosolic immunostaining. ×1000. **J:** Pancreas, demonstrating strong BAD immunostaining in association with perinuclear organelles in most of the exocrine cells. Pancreatic duct epithelium is immunonegative. ×400. **K:** Kidney, demonstrating strong BAD immunostaining in association with organelles in the epithelial cells lining the thin loops of Henle, distal convoluted tubule, and collecting ducts. In the more proximal parts of the nephron, only faint or no cytosolic BAD immunostaining was observed. ×400. **L:** Oviduct, showing strong punctate BAD immunostaining in culiated cuboid/columnar epithelial cells, with only a faint component of diffuse cytosolic BAD staining. Connective tissue fibroblasts and endothelial cells are immunonegative. ×400. **M:** Bone marrow, demonstrating strong BAD immunostaining located diffusely through the cytosol in most mature granulocytes, bands, and monocytes. ×1000. **N:** Staining of bone marrow with control mouse IgG from the same paraffin block. **O:** Reactive lymph node, showing prominent BAD immunostaining in plasma cells located in a germinal center (GC) and surrounding interfollicular area (right). Small lymphocytes are BAD immunonegative, whereas lymphoblasts and histiocytes often contain weak intensity diffuse cytosolic BAD immunostaining. ×250. **P:** Negative control immunostaining of the same node. ×150. Q. Dorsal root ganglion, showing strong BAD immunoreactivity in association with mitochondria in most but not all of the dorsal root ganglion neurons. Note the donut-like immunostaining of these organelles, suggesting association with the outer rather than inner mitochondrial membrane. These cells also contain lipofuscin granules, which can give the false impression of weakly immunostained organelles in some cells. Note that surrounding satellite cells and fibroblasts are immunonegative. ×400.

Table 2. BAD Protein Expression in the National Cancer Institute Anti-Cancer Drug Screening Panel of Tumor Cell Lines

Cell line	Score
Breast	
BT-549	0
HS578T	++
MCF-7	++
MCF7 ADR/RES	+/0
MDA-MB-231	0
MDA-MB-435	+
MDA-N	+++
T47D	0
Colon	
COLO205	++++*
HCT-15	+
HCT-116	+++
HCC-2998	+++
HT29	++
KM-12	0
SW-620	+++
Gliomas	
SF-268	++
SF-295	+++
SF-539	0
SNB-19	+*
SNB-75	+++*
U251	+/0*
Leukemia/lymphoma	
CCRF-CEM	0
HL-60	0
K562	+/0
MOLT-4	0
RPMI-8226	0
RS11846	0
SR	0
Lung	
A549	+++
EKVX	+/0
HOP-62	++++
HOP-92	0
NCI-H322M	0
NCI-H226	++
NCI-H23	+++
NCI-H522	+/0
NCI-H460	+++
Melanoma	
LOX-IMVI	0
MALME-3M	+*
M14	+++
SK-MEL-2	++
SK-MEL-5	+++
SK-MEL-28	+++*
UACC-62	++
UACC-257	+++*
Ovarian	
IGROV-1	+
OVCAR-3	0
OVCAR-4	0
OVCAR-5	+++
OVCAR-8	+
SK-OV-3	0
Prostate	
DU-145	+++
PC-3	+/0
Renal	
786-0	0
A498	++*
ACHN	+/0
CAKI-1	+/0
RXF-393	+/0
SN12C	+*
TK-10	+++*
UO-31	+/0

Data represent estimated BAD protein levels (ng per 50 μg of total protein) based on quantification of immunoblot data by densitometric scanning and extrapolation from a GST-BAD standard curve. In addition to the National Cancer Institute 60-cell-line drug screening panel, the B cell lymphoma line RS11846 was included. Data were scored as follows: 0, undetectable; +/−, 1 to ≤5 ng/50 μg; +, 5 to ≤10 ng/50 μg; ++, 10 to ≤15 ng/50 μg; +++, 15 to ≤20 ng/50 μg; and ++++, >20 ng/50 μg). Tumor lines are grouped by categories.

*Tumor cell lines that contained both hyperphosphorylated and normal BAD protein bands.

136, which reside within a consensus motif RXRXXS for 14-3-3 binding.[7] Analogous motifs are also found in the human BAD protein. Mutational analysis of these two serines suggests that phosphorylation of either or both of these amino acid residues impairs the ability of BAD to bind Bcl-X_L and diminishes the BAD protein's pro-apoptotic activity, with simultaneous phosphorylation at both serines representing a more fully inactive form than BAD phosphorylated at only one site.[7] As only the hyperphosphorylated form of BAD where both serines are phosphorylated migrates with clearly reduced mobility in SDS-PAGE experiments,[7] it is likely that our immunoblot analysis underestimated the extent to which the BAD protein is phosphorylated in human tumor cell lines.

These technical issues aside, it is important to recognize that the factors that lead to BAD phosphorylation or dephosphorylation in tumors *in vivo* may not be recapitulated *in vitro* under the usual culture conditions used for maintaining these cell lines. Thus, the data presented here revealing a doublet of BAD bands in some types of tumor lines and a single band in most should not be taken as evidence that BAD is either phosphorylated or dephosphorylated in particular types of cancers *in vivo*. The results do, however, suggest that some types of human tumor lines have a tendency to express relatively high levels of BAD protein (such as cancers of the colon, lung, and prostate and melanomas) whereas others (such as leukemias and lymphomas) typically contain little or no BAD. It remains to be determined whether the absence of BAD protein observed for some tumor lines represents an aberrant loss of BAD expression relative to the corresponding normal tissues.

The immunolocalization of BAD protein in many normal human tissues suggests association of this pro-apoptotic protein with mitochondria. Presumably, therefore, in these tissues, BAD is mostly in a dephosphorylated state that allows it to dimerize with anti-apoptotic Bcl-2 family proteins such as Bcl-2 and Bcl-X_L. Exceptions, however, were found among leukocytes, plasma cells, keratinocytes, chondrocytes, esophageal epithelium, and some other types of cells where the immunostaining was mostly present throughout the cytosol. In those circumstances, it seems probable that BAD is phosphorylated and thus targeted to the cytosol, although formal proof of this must await biochemical characterization of the phosphorylation status of the BAD protein in those particular types of cells. It will also be of interest in future studies to contrast the immunolocalization of BAD in normal tissues where mitochondrial association was found with tumors derived from those same tissues, inquiring whether signal transduction pathways have been activated that lead to redistribution of BAD in tumors.

Acknowledgments

We thank Xiao-kun Xiao for technical assistance and H. Gallant for manuscript preparation.

References

1. Reed JC: Bcl-2 and the regulation of programmed cell death. J Cell Biol 1994, 124:1–6
2. Thompson CB: Apoptosis in the pathogenesis and treatment of disease. Science 1995, 267:1456–1462
3. Ruoslahti E, Reed JC: Anchorage dependence, integrins, and apoptosis. Cell 1994, 77:477–478
4. Yang E, Korsmeyer SJ: Molecular thanatopsis: a discourse on the Bcl2 family and cell death. Blood 1996, 88:386–401
5. Yang E, Jockel J, Zha J, Korsmeyer S: Bad, a new bcl-2 family member, heterodimerizes with bcl-2 and bcl-XL in vivo and promotes cell death. Blood 1994, 84(suppl 1):373a
6. Yang E, Zha J, Jockel J, Boise LH, Thompson CB, Korsmeyer SJ: Bad, a heterodimeric partner for Bcl-XL and Bcl-2, displaces bax and promotes cell death. Cell 1995, 80:285–291
7. Zha J, Harada H, Yang E, Jockel J, Korsmeyer SJ: Serine phosphorylation of death agonist BAD in response to survival factor results in binding to 14-3-3 not BCL-X_L. Cell 1996, 87:619–628
8. Datta SR, Dudek H, Tao X, Masters S, Fu H, Gotoh Y, Greenberg ME: Akt phosphorylation of BAD couples survival signals to the cell-intrinsic death machinery. Cell 1997, 91:231–241
9. Wang HG, Rapp UR, Reed JC: Bcl-2 targets the protein kinase Raf-1 to mitochondria. Cell 1996, 87:629–638
10. Katsumata M, Siegel RM, Louie DC, Miyashita T, Tsujimoto Y, Nowell PC, Greene MI, Reed JC: Differential effects of Bcl-2 on T and B cells in transgenic mice. Proc Natl Acad Sci USA 1992, 89:11376–11380
11. Reed JC, Tanaka S, Cuddy M, Cho D, Smith J, Kallen R, Saragovi HU, Torigoe T: A strategy for generating monoclonal antibodies against recombinant baculovirus-produced proteins: application to the Bcl-2 oncoprotein. Anal Biochem 1992, 205:70–76
12. Krajewski S, Krajewska M, Shabaik A, Wang H-G, Irie S, Fong L, Reed JC: Immunohistochemical analysis of in vivo patterns of Bcl-X expression. Cancer Res 1994, 54:5501–5507
13. Krajewski S, Bodrug S, Krajewska M, Shabaik A, Gascoyne R, Berean K, Reed JC: Immunohistochemical analysis of Mcl-1 protein in human tissues: differential regulation of Mcl-1 and Bcl-2 protein production suggests a unique role for Mcl-1 in control of programmed cell death *in vivo*. Am J Pathol 1995, 146:1309–1319
14. Krajewski S, Krajewska M, Reed JC: Immunohistochemical analysis of in vivo patterns of Bak expression, a pro-apoptotic member of the Bcl-2 protein family. Cancer Res 1996, 56:2849–2855
15. Lee JS, Paull K, Alvarez M, Hose C, Monks A, Grever M, Fojo AT, Bates SE: Rhodamine efflux patterns predict P-glycoprotein substrates in the National Cancer Institute drug screen. Mol Pharmacol 1994, 46:627–638